DOI:

Article type: Full Paper

Development of High Power Density Metal-Supported Solid Oxide Fuel Cells

Michael C. Tucker *

Dr. M. C. Tucker

Lawrence Berkeley National Laboratory, 1 Cyclotron Rd, Berkeley, CA 94720 USA

E-mail: MCTucker@LBL.gov

Keywords: fuel cells,

Symmetric metal-supported solid oxide fuel cells (MS-SOFC) are fabricated with infiltrated catalysts on both anode and cathode side. Various aspects of the infiltration process are optimized. Performance is found to be quite sensitive to precursor dilution, catalyst loading, and catalyst calcining temperature. For an optimized cell with LSM cathode and SDCN anode, peak power density of 0.44, 1.1, and 1.9 W cm-2 at 600°C, 700°C and 800°C, respectively is achieved. A fully symmetric MS-SOFC with SDCN on both the anode and cathode sides achieves moderate peak power density of 0.12, 0.37 and 0.76 W cm-2 at 600°C, 700°C, and 800°C, respectively. A novel solvent-based infiltration technique is also explored, and found to be more effective than capillary forces alone, but not as effective as vacuum-infiltration.

1. Introduction

Metal-supported solid oxide fuel cells (MS-SOFC) display a number of advantages over conventional all-ceramic SOFCs, including low-cost structural materials (e.g. stainless steel), mechanical ruggedness, excellent tolerance to redox cycling, and extremely fast start-up capability. Challenges for MS-SOFCs

include: oxidation of the metal support, especially at 800°C and higher; the possibility of the stainless steel exacerbating Cr poisoning of the cathode catalyst; fabrication and materials set restrictions arising from the requirement that stainless steel be sintered in reducing atmosphere; and, only moderate performance and lifetime have been demonstrated to date. These issues, and various approaches to overcome the challenges, have been discussed in detail in the literature.[1–5]

These advantages and challenges suggest that MS-SOFCs may be well-suited for portable, ruggedized, fast-start, intermittent-fuel, or other unique and innovative applications. MS-SOFC stacks have been developed for direct placement in charcoal cooking stoves,[6,7] home-scale combined heat and power,[8] and propane-fueled personal device chargers,[9] all applications where conventional all-ceramic SOFCs have limitations. Nissan has developed the world's first light-duty prototype vehicle with a conventional SOFC stack for cruising range extension, fueled by bio-ethanol reformate.[10] Because of the desire for rapid-start capability, developing MS-SOFC cell and stack technology for this vehicular application is a priority. The small volume allowance for the SOFC stack on-board a small vehicle furthermore demands high power density from the MS-SOFC.

This work is an extension of our previous efforts developing co-sintered, YSZ-based MS-SOFCs with porous metal supports on both anode and cathode sides, and catalysts deposited into both electrodes via infiltration.[11–14] These features provide for a mechanically rugged cell that can be processed with low-cost scalable techniques, and high surface-area catalysts that provide excellent performance by avoiding interdiffusion or coarsening during cell sintering.[1] To support the vehicular traction application, in this work we further develop catalyst infiltration processing for MS-SOFCs to dramatically increase power density. The goal is to increase cell performance by improving infiltration of conventional catalyst compositions (lanthanum strontium manganite (LSM), Ni, doped ceria) into electrode backbones of conventional yttria-stabilized zirconia (YSZ). This is accomplished by optimizing various aspects of the infiltration process, including precursor composition, catalyst loading, crystallization temperature, and method of introducing the precursor into the porous electrode backbone. Selection of an improved active material composition set will be the subject of future work.

2. Results and Discussion

2.1 Cell structure

The metal and YSZ backbone structure of the MS-SOFC, without catalysts infiltrated, is shown in Figure 1a-b. Cells are laser-cut from laminated tape-cast layers, and can be fabricated in a range of size and shape. Lab-scale cells of 30 mm diameter and 1 to 4 cm2 of active area with catalysts deposited are used throughout this work; as cell performance increased, smaller active area was used to keep maximum current within the limit of the potentiostat. Previous experiments indicated that cell performance is

independent of active are in this range. The cross-section SEM images reveal a highly porous metal support on both sides of the cell, surrounding thin active ceramic layers. The dense YSZ electrolyte layer is approximately 10 □m thick. Mechanical interlocking between the rough metal surface and porous YSZ electrode layers provides adequate bonding to maintain cell integrity. Suitable poreformer loading in the porous YSZ electrode layers allows infiltration of the catalyst throughout the layer and gas transport during operation, without sacrificing mechanical integrity of the electrode. Figure 1c shows LSM catalyst deposited within a pore in the YSZ electrode layer. The LSM adheres to the pore wall, leaving pore space open for gas transport. The primary catalyst particles are about 50 to 100 nm in size.

As can be seen clearly in Fig. 1, the stainless steel and YSZ cell architecture is symmetric. This means that small differences in sintering rate or coefficient of thermal expansion between the stainless steel and YSZ do not lead to warping of the cell. We anticipate this will be an advantage for deployment of large MS-SOFC stacks, where large thermal gradients can be expected during fabrication and operation.

2.2 Baseline performance

A baseline cell with LSM cathode and YDC-Ni [80:20] anode was prepared using our existing standard infiltration technique. The choice to use an anode composition with doped ceria and minimal Ni arises from the rapid coarsening observed for infiltrated Ni in hydrogen fuel.[12] The performance with hydrogen fuel is shown in Figure 2. Every 100°C of increased operation temperature leads to roughly a doubling of power density. The performance is similar to previous tubular cells operated with air and hydrogen with Ni anode catalyst,[13] and 5 times better than similar planar cells operated with charcoal fuel, where gasification of the charcoal to H2 and CO limited cell performance.[7] The linear polarization curve suggests minimal activation or mass transport overpotentials.

2.3 Infiltration process development

To improve performance beyond that shown in Section 2.2, we undertook a systematic variation of several features of the infiltration process. The intention is to identify those features that have a large impact on cell performance, and optimize them.

2.3.1 Precursor solution composition

The catalyst precursor salts melt in the range 37-96°C (except Sr-nitrate which must be dissolved), allowing a highly concentrated molten salt bath to be prepared by heating to around 100°C.[15] Addition of water to the salt mixture, however, greatly enhances the ability to make a clear, low-viscosity, low surface-tension solution that remains a liquid over a larger temperature range, making it

easier to infiltrate into the cell. The trade-off is that water addition dilutes the precursor, resulting in less catalyst deposited within the cell for each infiltration cycle. Precursors with 20 wt% additional water ("Concentrated") and 100 wt% additional water ("Diluted") were assessed. As shown in Figure 3, the best performance was found for concentrated LSM and diluted YDCN. This is consistent with the observation that LSM precursor melts around 65°C (far below the infiltration temperature of 90°C) so excess water is not needed to keep it from solidifying. In contrast, dry YDCN precursor melts around 85°C, so it can easily crystallize before infiltration is complete if the cell cools a few degrees. We later found that 40 wt% water addition to the YDCN anode precursor is sufficient to prevent crystallization during infiltration, so this was used for optimized cell fabrication.

Previous work at LBNL used Sm-doped ceria (SDC), whereas Y-doped ceria (YDC) was used at Point Source Power. Both dopants were compared here, and the results are shown in Supporting Information, Figure S1. SDC provided marginally higher performance, so it was selected for all later cell fabrications. Infiltrated Ni is known to coarsen quickly during operation,[12] and addition of doped ceria can stabilize the Ni and reduce degradation rate.[16] Previous work used SDC:Ni volume ratio of 80:20,[7] and that ratio is maintained here. A limited number of cells were also produced with a higher Ni content, the results of which are shown in the Supporting Information.

2.3.2 Crystallization temperature

The nitrate precursors convert to oxides around 230°C and crystallize around 560°C.[17] Cells are heated to 600°C or higher to ensure complete conversion to the desired phase. During cell development, we noticed that the ohmic impedance of a LSM/LSM symmetric cell improved after operation in air at 850°C, as shown in Figure 4a and b. We surmise that higher temperature leads to improved crystallization or particle-to-particle sintered connection of the catalysts, leading to increased electronic conductivity. Higher temperature also leads to coarsening of the catalysts,[12] resulting in lower surface area and significantly higher electrode polarization impedance as can be seen in Figure 4b. Based on this hypothesis, cells were fabricated with either the first cathode, or both the first anode and first cathode infiltrations heated to 850°C to provide a good electronic network, followed by subsequent infiltrations heated to 600°C to provide high surface area. The intended impact on conductivity was achieved: ohmic impedance was 0.89, 0.55, and 0.50 Ohm*cm2 for neither, cathode, and both electrode first infiltrations heated to 850°C, respectively. As shown in Figure 4c, treating both the anode and cathode first infiltrations at high temperature significantly improved performance.

2.3.3 Catalyst loading

The amount of catalyst introduced by each infiltration cycle can be estimated from the precursor and catalyst densities, assuming complete flooding of the pores with catalyst precursor. The filling factors

are low: for Ni, SDC, and LSM, 3, 10, and 15% respectively of the pore volume is filled with catalyst for each infiltration cycle. Addition of water further reduces these filling factors. Because of these low filling factors, it is desirable to infiltrate multiple times to increase catalyst loading. At low loading, low catalyst surface area and poor electronic connection between catalyst particles limits performance. At high loading, pore filling may limit mass transport, and cost increases. To demonstrate the impact of catalyst loading on performance, the cell power and AC impedance components at 700°C are shown in Figure 5 as a function of the number of infiltration cycles. The ohmic impedance decreases moderately with increasing infiltrations as electronic percolation improves. For both LSM and SDCN, electrode polarization impedance drops dramatically up to 3 infiltrations, and then plateaus for more infiltrations in the range studied. Therefore, 3x was selected as the optimum to balance high performance and catalyst consumption.

2.4 Vacuum-free infiltration

Application of mild vacuum to the cells during infiltration is common.[18] This helps remove air from the porous structure, ensuring complete filling of the pores with catalyst precursor in the event that capillary wetting forces are not sufficient. Application of vacuum, however, is time consuming, removes water from the precursor solution (thereby changing the concentration), and adds cost to the production process. We previously proposed an alternative solvent-assisted vacuum-free process wherein a solvent with low boiling point and low surface tension (e.g. ethanol, acetone, etc.) is flooded into the pores before the cell is submerged in the catalyst precursor bath.[19] Upon contacting the hot precursor solution, the solvent boils off and evacuates the pores, thereby promoting flooding of the pores by precursor. We apply that technique here to assess its suitability for a processing scheme with the goal of high cell power density.

Figure 6 shows the peak power density achieved for cells processed with the solvent-assisted infiltration procedure, and standard procedure developed in the previous sections. Also shown is performance of a baseline cell that had neither vacuum nor solvent applied, but rather was simply dipped and held in the precursor bath for the standard time, about 10 sec. Both the solvent and vacuum techniques provided substantially higher performance than the simple dipping. Although capillary forces are quite strong and can be expected to completely flood a cell dipped into a well-wetting solution, it is clear that the viscous, highly concentrated solutions we use to minimize repetition of the infiltration procedure require extra measures to completely flood the pores. Although the solvent-assisted infiltration procedure is promising and may benefit from further development, it did not exceed the standard vacuum-assisted process and so was not pursued further in this work.

2.5 Performance of optimized cells

Optimized cells were fabricated using the best infiltration practices determined in Section 2.3 and 2.4: LSM with 20 wt% water added and SDCN with 40 wt% water added; SDCN rather than YDCN; both anode and cathode heated to 850°C on the first infiltration cycle, and then 600°C on subsequent cycles; three infiltration cycles total for each side of the cell; and, vacuum-assisted infiltration. The resulting cell performance is shown in Figure 7a. Dramatic improvement was achieved relative to the baseline performance shown in Figure 2. The 1.9 W cm-2 obtained at 800°C is the highest power density reported for stainless-steel-supported SOFCs to date (slightly higher power was reported for a cell with LSGM electrolyte deposited on Fe-Ni substrate)[20]. These results clearly indicate the importance of optimizing and controlling the infiltration procedure, and we expect that the improvements identified here will not introduce significant additional cost, if any. Furthermore, these improvements were achieved with longstanding conventional SOFC active materials (YSZ, LSM, doped ceria, and Ni). Further improvement via substitution of these materials by higher-performance materials reporte more recently is the subject of future work.

Figure 7b shows performance for a completely symmetric cell, in which not only is the YSZ and stainless steel structure symmetric, but SDCN is used as the catalyst for both the anode and cathode as well. This approach was used at Point Source Power to make infiltration simpler (the cell can be dunked in a precursor bath without any masking), remove the need for tracking which side of the cell is which during stack assembly, and overcome rapid degradation of the LSM via Cr contamination in the presence of K-containing biomass fuel.[6,7,21] More recently, symmetric MS-SOFCs with infiltrated $La_{0.6}Sr_{0.4}Fe_{0.9}Sc_{0.1}O_{3-\delta}$ (LSFSc) on both sides achieved 0.3 and 0.65 W cm-2 at 700°C and 800°C, respectively.[22] The performance obtained here for symmetric SDCN is slightly higher, at 0.37 and 0.76 W cm-2 at 700°C and 800°C, respectively, and is among the highest ever reported for symmetric SOFCs of any type.[23,24] The precise mechanism of SDCN cathode catalysis is not yet clear, and its high performance deserves further investigation. It has been noted, however, that nano-scale doped ceria can present mixed conduction in air due to the large influence of grain boundary relative to bulk.[25] Of course, LSM is a much better cathode catalyst than SDCN as clearly seen in Figure 7c, but a symmetric cell with moderate power density may be interesting for some applications.[23,26]

AC impedance spectra for the optimized LSM-SDCN and symmetric-SDCN cells are shown in Figure 8a-b. Electrode polarization impedance dominates the total impedance, suggesting catalyst development would be fruitful to achieve further performance improvement. The ohmic impedance is shown in Figure 8c. For a cell with high Ni content in the anode (SDC 20v%-Ni 80v%, discussed in Supporting Information, Figure S2), the total cell ohmic impedance is similar to the theoretical value for the 10 μm-thick YSZ electrolyte layer, indicating excellent electronic conduction in both electrodes. In contrast, the ohmic impedance is roughly twice as high for the optimized cell with only 20v% Ni, consistent with the lower electronic conductivity of SDC relative to Ni. The symmetric cell has significantly higher ohmic impedance, as high-conductivity LSM is replaced with SDCN; both SDC and Ni-oxide have relatively low electronic conductivity in air.

3. Conclusion

Symmetric-architecture metal-supported solid oxide fuel cells were fabricated with infiltrated catalysts on both anode and cathode side. Various aspects of the infiltration process were addressed to maximize performance. Performance was found to be quite sensitive to precursor dilution, catalyst loading, and catalyst calcining temperature. Performance was relatively insensitive to the type of ceria dopant and ceria-to-nickel ratio. It was found that capillary forces are sufficient to introduce some catalyst into the electrodes, however, addition of vacuum-assisted processing during infiltration greatly improves performance. A novel solvent-assisted infiltration technique was also used, and found to be more effective than capillary forces alone, but not as effective as vacuum-infiltration. For an optimized cell with LSM cathode and SDCN anode, peak power density of 0.44, 1.1, and 1.9 W cm-2 at 600°C, 700°C and 800°C, respectively was achieved. This is about 450% higher power than was observed for the baseline cell before the infiltration process was optimized, and is the highest power density reported for stainless-steel-supported SOFCs to date. A fully symmetric MS-SOFC with SDCN on both the anode and cathode sides achieved peak power density of 0.12, 0.37 and 0.76 W cm-2 at 600°C, 700°C, and 800°C, respectively, and is among the highest performance reported for symmetric SOFCs of any type. Demonstrating rapid thermal cycling, redox tolerance, and lifetime durability for the high-power cells developed here is the subject of ongoing work.

4. Experimental Section

Green cells were assembled by laminating individual YSZ (8Y, Tosoh) or stainless steel (P434L alloy, water atomized, Ametek Specialty Metal Products) layers prepared by tape-casting. The layers were prepared with polymethyl methacrylate poreformer beads (Esprix Technologies) and water-based tape-casting binder. Individual cells were cut from a larger green sheet with a laser cutter (Hobby model, Full Spectrum Laser). Cells were then debinded by firing in air in a box furnace at 525°C for 1 h with 0.5°C min-1 heat-up rate to slowly remove the binder and poreformer. Cells were sintered at 1350°C for 2h in a tube furnace with flowing 2% hydrogen in argon.

After sintering, cells were infiltrated by techniques described previously [13,15] with La0.15Sr0.85MnO3-d (LSM) on the cathode side and Sm0.2Ce0.8O2-d (SDC) or Y0.2Ce0.8O2-d (YDC) mixed with Ni on the anode side (SDCN or YDCN). The ceria:Ni volume ratio was 80:20, except as noted. Precursor mixtures of metal nitrates (Sigma Aldrich) were prepared with the intended final stoichiometric composition, with Triton-X surfactant (Sigma Aldrich, at surfactant loading of 0.3 g per 2 g of resulting catalyst particles) and 20 to 100 wt% water added to improve wetting into the cell pores.

The precursor mixture was heated to ~90°C, the cell was submerged into it, and then mild vacuum was applied to evacuate the cell pores. Areas of the cell that were not intended to be infiltrated were coated with acrylic paint mask (Liquitex). In certain cases, the vacuum was not applied, and the cells were simply dipped into the hot precursor solution. Cells with “solvent-assisted” infiltration were flooded with acetone before being dipped into the precursor solution. The acetone rapidly boils and evacuates the cell pores, promoting infiltration of the precursor throughout the porous structure. No external vacuum was applied in this case. After introducing the precursor into the cell, it was fired with a 3°C min-1 heating rate to 600 or 850°C for 30 min in air to convert the precursor to the intended oxide phases. Any loose catalyst was removed from the surface of the cell by light brushing. Cells were re-infiltrated a number of times (noted in the figure captions, for example 2x is two infiltrations) before operation and testing.

Complete cells were mounted to an alumina tube test rig using ceramic adhesive paste (Aremco 552), with the anode side facing the inside of the tube. Each side of the cell was contacted with two platinum wires, attached with a small piece of platinum mesh spot-welded to the wire and the cell. Cells were heated at 5°C min-1 to the operating temperature, with ambient air outside the tube, and hydrogen bubbled through water at room temperature flowing at 120 cm3 min-1 through the inside of the tube. Open circuit voltage (OCV), current-step I-V polarization, and AC impedance (at OCV, 200 kHz to 0.1 Hz) were recorded with a multichannel potentiostat and current booster (Biologic).

Supporting Information

Supporting Information is available from the Wiley Online Library or from the author.

Acknowledgements

The author acknowledges Grace Lau for assistance with sintering the cells used in this work. Funding for this work was provided by Nissan Motor Co., Ltd. through Strategic Partnership Projects Agreement FP00002581. This work was funded in part by the U.S. Department of Energy under contract no. DE-AC02-05CH11231.

Received: ((will be filled in by the editorial staff))

Revised: ((will be filled in by the editorial staff))

Published online: ((will be filled in by the editorial staff))

References

[1] M. C. Tucker, J. Power Sources 2010, 195, 4570.

[2] Y. Larring, M.-L. Fontaine, Green Energy Technol. 2013, 55, 71.

[3] A. M. Dayaghi, K. J. Kim, S. J. Kim, J. Park, S. J. Kim, B. H. Park, G. M. Choi, J. Power Sources 2016, 324, 288.

[4] T. Franco, M. Haydn, A. Weber, W. Schafbauer, L. Blum, U. Packbier, D. Roehrens, N.H. Menzler, J. Rechberger, A. Venskutonis, L. S. Sigl, H.P. Buchkremer, ECS Trans. 2013, 57, 471.

[5] V. V. Krishnan, Wiley Interdiscip. Rev. Energy Environ. 2017, e246. doi: 10.1002/wene.246.

[6] M. Tucker, B. Carreon, J. Charyasatit, K. Langston, C. Taylor, J. Manjarrez, N. Burton, M. Labarbera, C. P. Jacobson, ECS Trans. 2013, 57, 503.

[7] M. C. Tucker, C. Taylor, M. LaBarbera, C. P. Jacobson, ECS Trans. 2013, 57, 2929.

[8] N. P. Brandon, D. Corcoran, D. Cummins, A. Duckett, K. EI-Khoury, D. Haigh, R. Leah, G. Lewis, N. Maynard, T. McColm, R. Trezona, A. Selcuk, M. Schmidt, J. Mater. Eng. Perform. 2004, 13, 253.

[9] Kraftwerk, Kickstarter campaign for mobile device charger using tubular metal-supported SOFCs, https://www.kickstarter.com/projects/ezelleron/kraftwerk-highly-innovative-portable-power-plant/description, Accessed: March, 2017.

[10] Nissan, Press release describing e-Bio Fuel Cell SOFC-powered vehicle concept, https://www.youtube.com/watch?v=HF-eE8pRzMw; http://reports.nissan-global.com/EN/?p=17768; http://nissannews.com/releases/dcbe806e-6c8d-4079-a7c9-dd21a590b779/download/d5bf044d-18ea-4d73-a8b3-13e746f7f5ec?l=en-US, Accessed: March, 2017.

[11] M. C. Tucker, C. P. Jacobson, L. C. De Jonghe, S. J. Visco, J. Power Sources 2006, 160, 1049.

[12] M. C. Tucker, G. Y. Lau, C. P. Jacobson, L. C. DeJonghe, S. J. Visco, J. Power Sources 2008, 175, 447.

[13] M. C. Tucker, G. Y. Lau, C. P. Jacobson, L. C. DeJonghe, S. J. Visco, J. Power Sources 2007, 171, 477.

[14] Y. B. Matus, L. C. De Jonghe, C. P. Jacobson, S. J. Visco, Solid State Ionics 2005, 176, 443.

[15] T. Z. Sholklapper, V. Radmilovic, C. P. Jacobson, S. J. Visco, L. C. De Jonghe, Electrochem. Solid-State Lett. 2007, 10, B74.

[16] P. Blennow, J. Hjelm, T. Klemensoe, S. Ramousse, A. Kromp, A. Leonide, A. Weber, J. Power Sources 2011, 196, 7117.

[17] T. Z. Sholklapper, PhD Thesis, University of California at Berkeley, May 2007.

[18] S. P. Jiang, Int. J. Hydrogen Energy 2012, 37, 449.

[19] M. C. Tucker, T. Z. Sholklapper (The Regents Of The University Of California) US 2011/0251053A1, 2011.

[20] Y.-W. Ju, T. Inagaki, S. Ida, T. Ishihara, J. Electrochem. Soc. 2011, 158, B825.

[21] C. P. Jacobson, M. C. Tucker, T. Z. Sholklapper (Point Source Power, Inc.) US 2011/0111309A1, 2011.

[22] Y. Zhou, X. Liu, J. Li, H. Nie, X. Ye, S. Wang, Z. Zhan, J. Power Sources 2014, 252, 164.

[23] J. C. Ruiz-Morales, D. Marrero-López, J. Canales-Vázquez, J. T. S. Irvine, RSC Adv. 2011, 1, 1403.

[24] X. Liu, D. Han, Y. Zhou, X. Meng, H. Wu, J. Li, F. Zeng, Z. Zhan, J. Power Sources 2014, 246, 457.

[25] J. Santiso, M. Burriel, J. Solid State Electrochem. 2011, 15, 985.

[26] J. Zhou, T.-H. Shin, C. Ni, G. Chen, K. Wu, Y. Cheng, J. T. S. Irvine, Chem. Mater. 2016, 28, 2981.

Figure 1. SEM image of (a,b) polished cross section of MS-SOFC structure after sintering and before catalyst infiltration, and (c) cathode pore after infiltration of LSM.

Figure 2. Polarization performance of baseline cell with LSM 2x and YDCN 2x calcined at 600°C.

Figure 3. Impact of precursor concentration for LSM 2x and YDCN 2x with either 20 wt% additional water (dilute) or 100 wt% additional water (concentrated). LSM concentrated and YDCN dilute (black squares), both dilute (red circles), and both concentrated (blue triangles).

Figure 4. Impact of crystallization temperature. (a) Ohmic and electrode portions of the impedance during heat-up and cool-down of a symmetric cell with LSM 2x and air on both sides; (b) AC impedance spectra for this cell at 650°C before (blue line) and after (green line) heating to 850°C (red line). (c) Peak power for cells with LSM 2x and YDCN 2x where the first LSM infiltration (red circles), first LSM and

YDCN infiltrations (black squares), or neither (blue triangles) were heated to 850°C and subsequent infiltrations were heated to 600°C.

Figure 5. Impact of catalyst loading. Peak power (a,c) and impedance components at 700°C (b,d) for variation in the number of infiltrations of either LSM (a,b) or SDCN (c,d), with the other electrode held constant at 2x infiltrations.

Figure 6. Effect of vacuum-assisted (black squares) or acetone-assisted infiltration (red triangles), compared to cell simply dipped into the precursor solution (blue circles).

Figure 7. Polarization performance for optimized cells with (a) LSM 3x and SDCN 3x, and (b) symmetric SDCN 3x in both electrodes. (c) Comparison of peak power density for the optimized LSM-SDCN (red triangles) and symmetric-SDCN (blue circles) to results for the baseline cell of Figure 2 (gray squares).

Figure 8. AC impedance spectra for optimized cells with (a) LSM 3x and SDCN 3x, and (b) symmetric SDCN 3x in both electrodes. (c) Comparison of ohmic impedance for the optimized LSM-SDCN (red triangles), symmetric-SDCN (blue circles), and LSM-SDCN with high Ni content (80Ni-20SDC, cyan squares) to the theoretical value for 10mm YSZ electrolyte layer (black line).

Metal-supported solid oxide fuel cells are infiltrated with both anode and cathode catalysts, and the infiltration process is optimized. The cell YSZ and stainless steel backbone architecture is symmetric, and LSM/SDCN and symmetric SDCN catalyst configurations are examined. Both achieve unusually high power density: 1.9 W cm-2 for LSM cathode and 0.76 W cm-2 for SDCN cathode at 800°C.

M.C. Tucker*

Development of High Power Density Metal-Supported Solid Oxide Fuel Cells

Supporting Information

Development of High Power Density Metal-Supported Solid Oxide Fuel Cells

Michael C. Tucker*

Figure S1. Impact of ceria dopant on performance for 80% ceria, 20% Ni. Dopant: yttrium (red) or samarium (blue). Both anode and cathode were infiltrated twice.

Figure S2. Results for a high-Ni-content anode (20v% SDC, 80v% Ni). (a) Polarization curves and (b) AC impedance spectra for cell with anode infiltrated 9 times and cathode infiltrated 3 times. The impact of the number of anode infiltrations is shown in (c) peak power vs. temperature, and (d) components of the AC impedance spectra at 700°C.

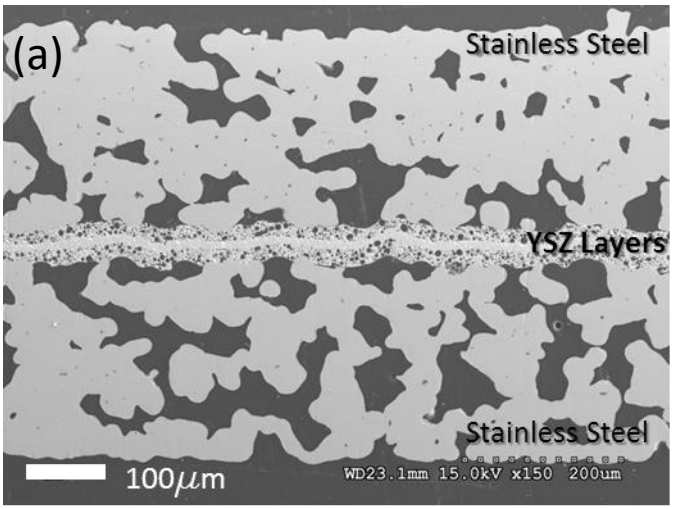
(a)
Stainless Steel
YSZ Layers
Stainless Steel
100μm
WD23.1mm 15.0kV x150 200um

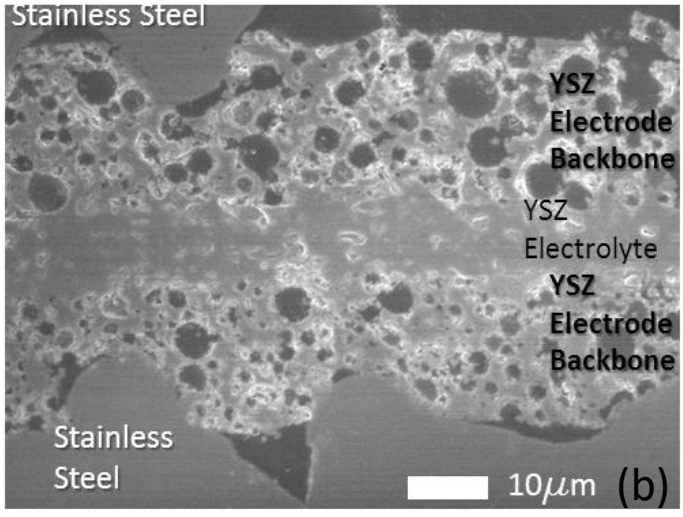
Stainless Steel
YSZ
Electrode
Backbone
YSZ
Electrolyte
YSZ
Electrode
Backbone
Stainless
Steel
10μm
(b)

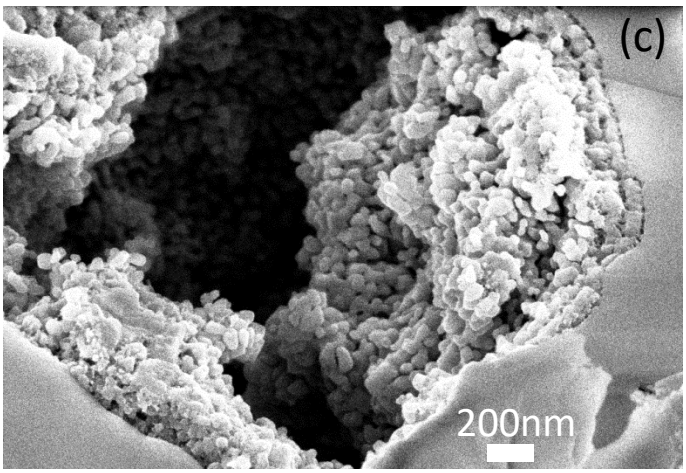
(c)
200nm

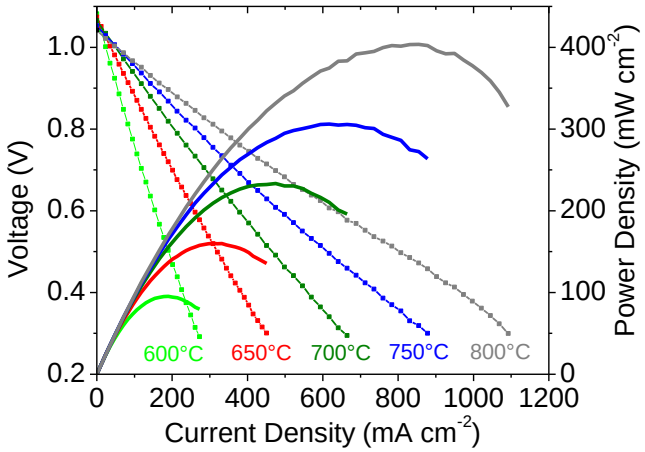
Voltage (V)
Power Density (mW cm-2)
Current Density (mA cm-2)
1.0
0.8
0.6
0.4
0.2
400
300
200
100
0
0
200
400
600
800
1000
1200
600°C
650°C
700°C
750°C
800°C

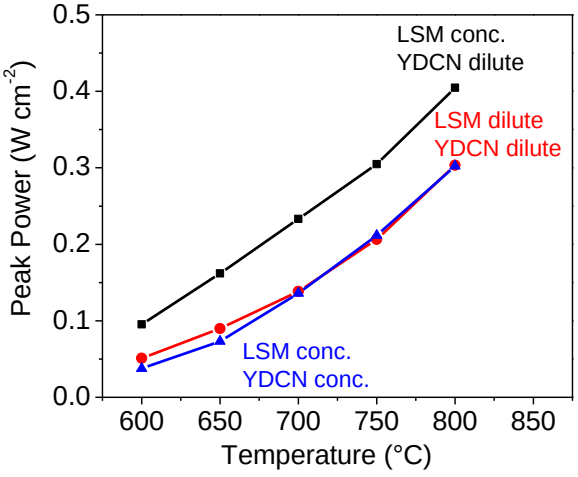
0.5
0.4
0.3
0.2
0.1
0.0
Peak Power (W cm-2)
600
650
700
750
800
850
Temperature (°C)
LSM conc.
YDCN dilute
LSM dilute
YDCN dilute
LSM conc.
YDCN conc.

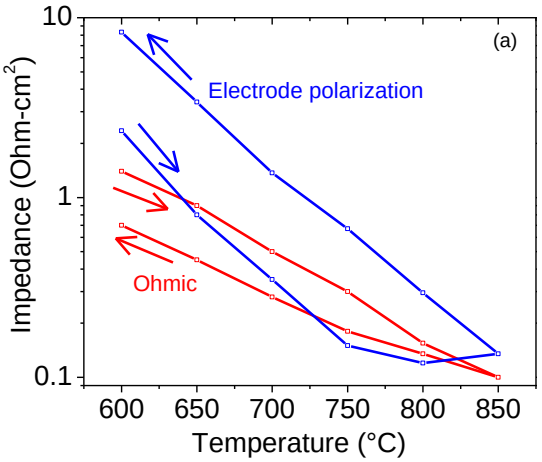
(a)
Electrode polarization
Ohmic
Impedance (Ohm-cm^2)
Temperature (°C)
10
1
0.1
600
650
700
750
800
850

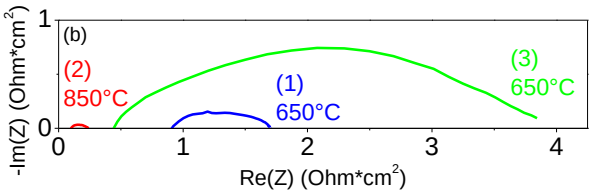
(b)
(2)
850°C
(1)
650°C
(3)
650°C
-Im(Z) (Ohm*cm^2)
Re(Z) (Ohm*cm^2)
0
1
2
3
4

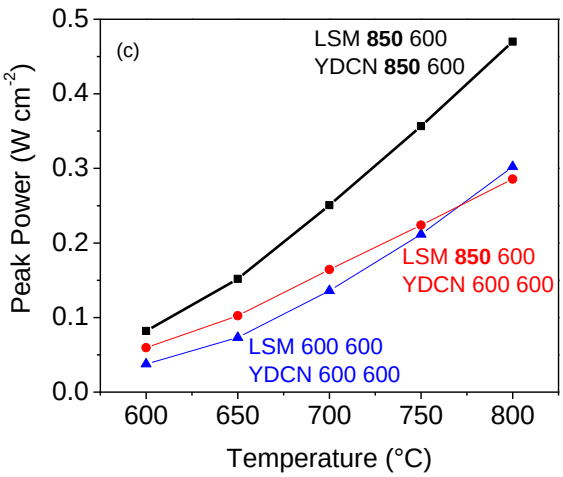
(c)
LSM **850** 600
YDCN **850** 600
LSM **850** 600
YDCN 600 600
LSM 600 600
YDCN 600 600
Peak Power (W cm^{-2})
Temperature (°C)
0.0
0.1
0.2
0.3
0.4
0.5
600
650
700
750
800

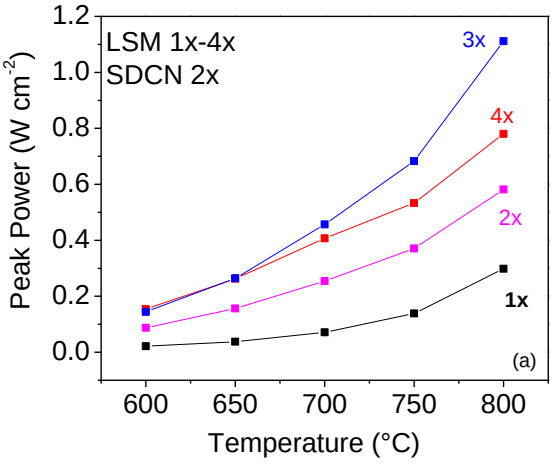
LSM 1x-4x
SDCN 2x
3x
4x
2x
1x
(a)
Peak Power (W cm-2)
Temperature (°C)
1.2
1.0
0.8
0.6
0.4
0.2
0.0
600
650
700
750
800

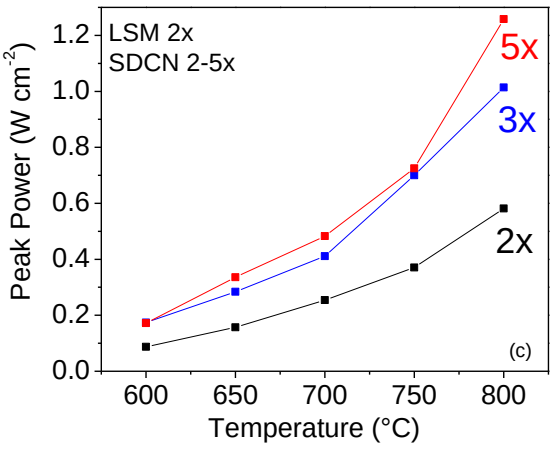
LSM 2x
SDCN 2-5x
5x
3x
2x
(c)
Peak Power (W cm-2)
Temperature (°C)
1.2
1.0
0.8
0.6
0.4
0.2
0.0
600
650
700
750
800

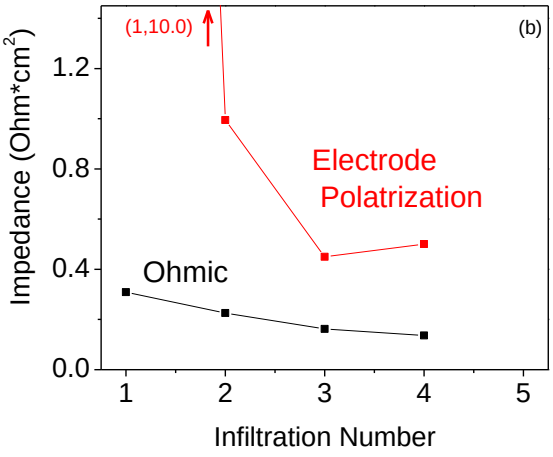
(1,10.0)
(b)
Electrode
Polatrization
Ohmic
Impedance (Ohm*cm2)
Infiltration Number
1.2
0.8
0.4
0.0
1
2
3
4
5

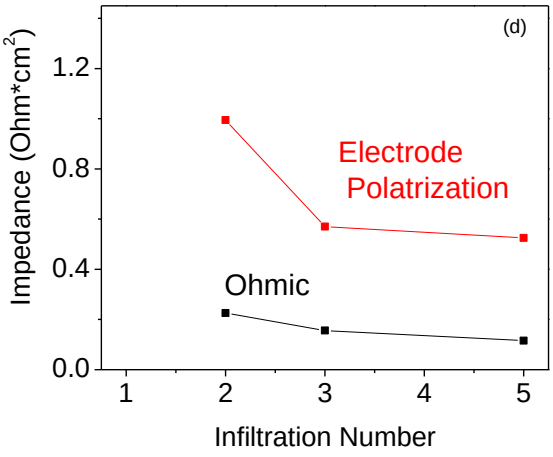
(d)
Electrode
Polatrization
Ohmic
Impedance (Ohm*cm2)
Infiltration Number
1.2
0.8
0.4
0.0
1
2
3
4
5

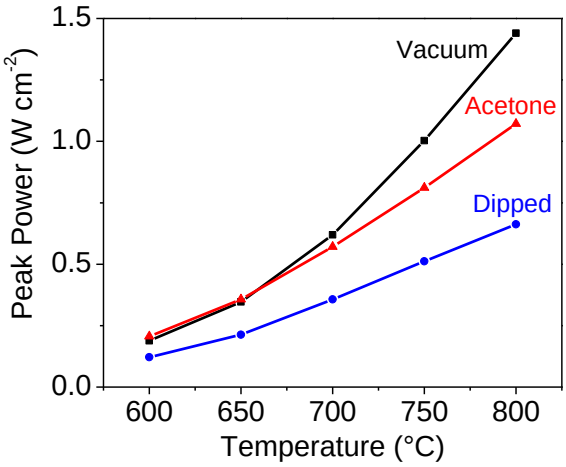
1.5
1.0
0.5
0.0
Peak Power (W cm-2)
600
650
700
750
800
Temperature (°C)
Vacuum
Acetone
Dipped

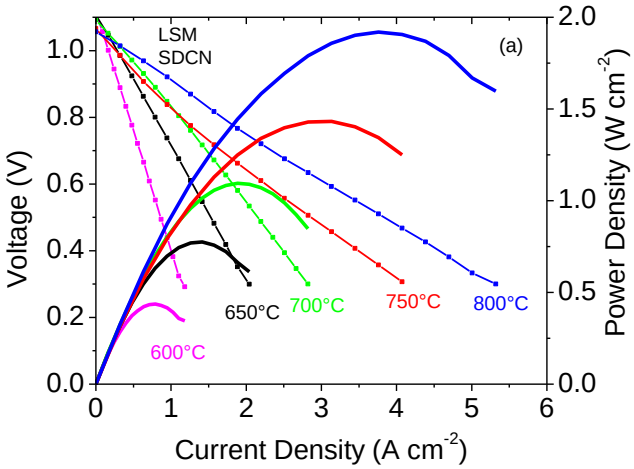
LSM
SDCN
(a)
650°C
700°C
750°C
800°C
600°C
Voltage (V)
Power Density (W cm-2)
Current Density (A cm-2)

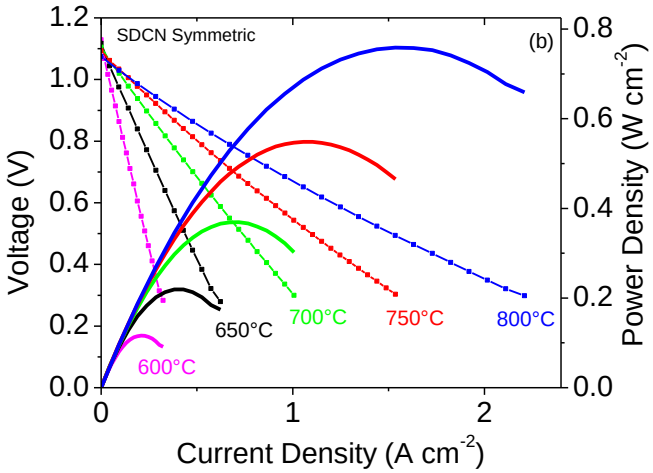
SDCN Symmetric
(b)
650°C
700°C
750°C
800°C
600°C
Voltage (V)
Power Density (W cm-2)
Current Density (A cm-2)

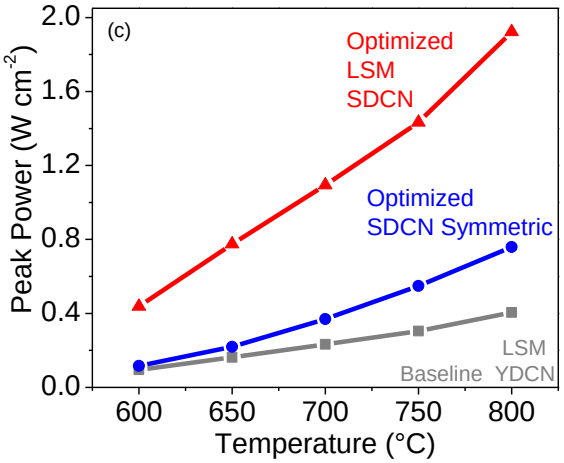
(c)
Optimized
LSM
SDCN
Optimized
SDCN Symmetric
LSM
Baseline YDCN
Peak Power (W cm-2)
Temperature (°C)

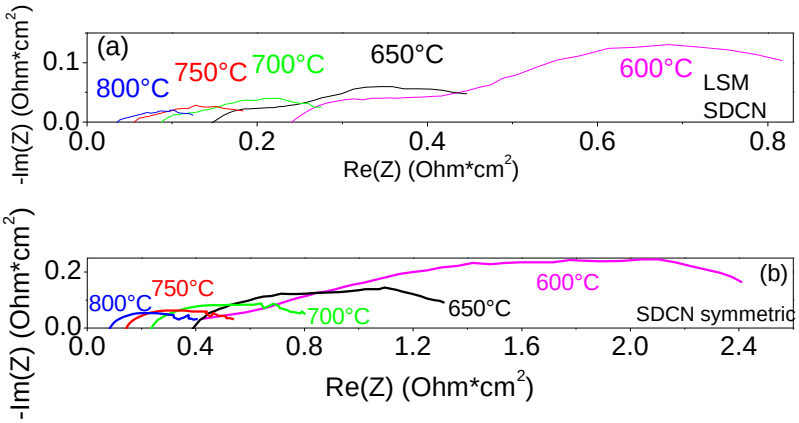
(a)
800°C
750°C
700°C
650°C
600°C
LSM
SDCN
-Im(Z) (Ohm*cm2)
Re(Z) (Ohm*cm2)
0.0
0.1
0.2
0.4
0.6
0.8
(b)
800°C
750°C
700°C
650°C
600°C
SDCN symmetric
-Im(Z) (Ohm*cm2)
Re(Z) (Ohm*cm2)
0.0
0.2
0.4
0.8
1.2
1.6
2.0
2.4

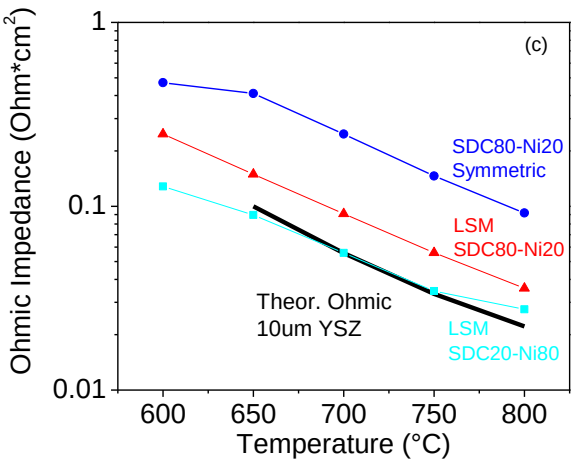
(c)
SDC80-Ni20
Symmetric
LSM
SDC80-Ni20
Theor. Ohmic
10um YSZ
LSM
SDC20-Ni80
Ohmic Impedance (Ohm*cm2)
Temperature (°C)
1
0.1
0.01
600
650
700
750
800

Supporting Information

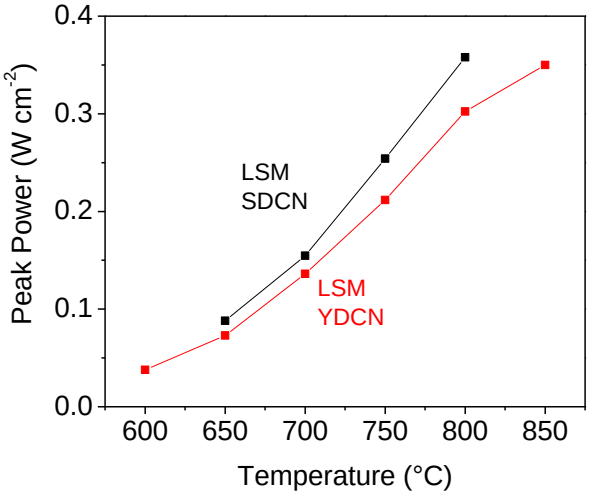

Figure S1. Impact of ceria dopant on performance for 80% ceria, 20% Ni. Dopant: yttrium (red) or samarium (blue). Both anode and cathode were infiltrated twice.

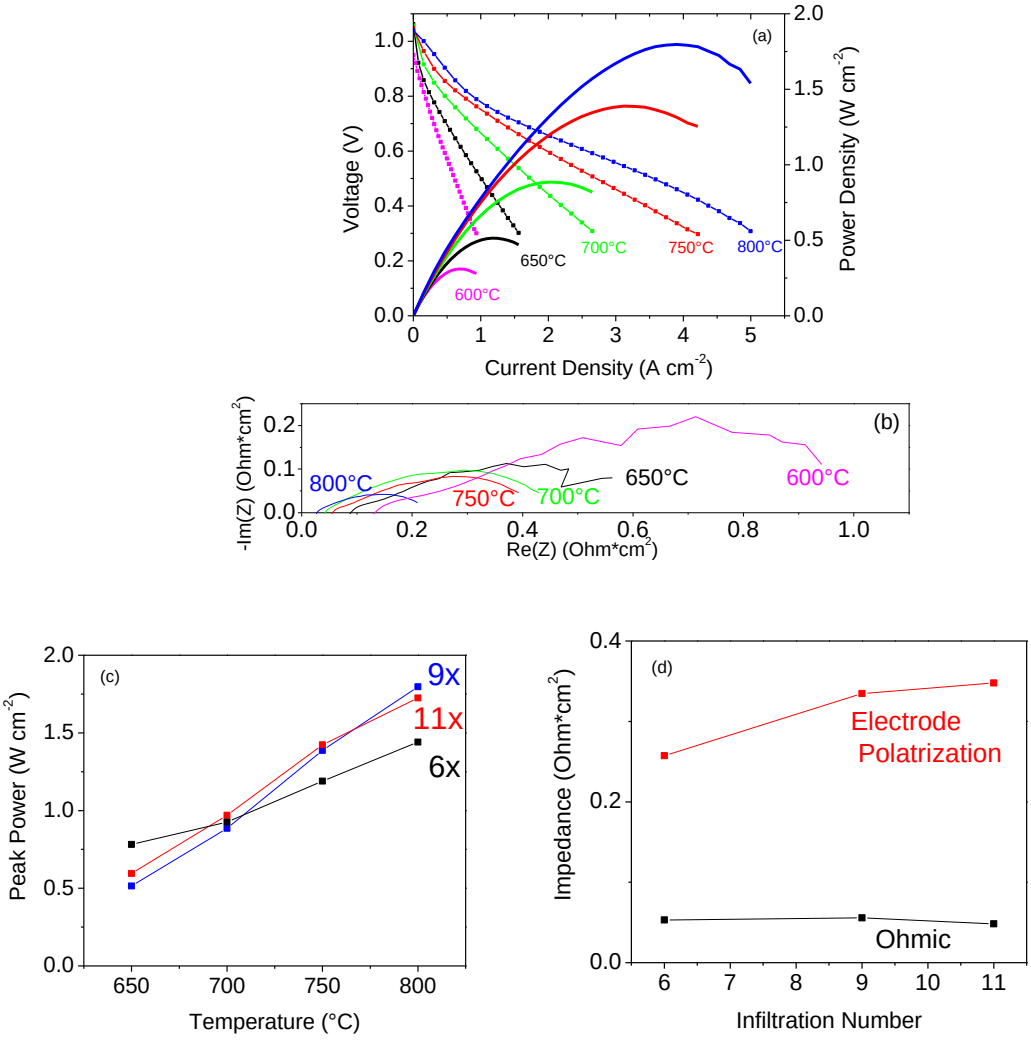

Figure S2. Results for a high-Ni-content anode (20v% SDC, 80v% Ni). (a) Polarization curves and (b) AC impedance spectra for cell with anode infiltrated 9 times and cathode infiltrated 3 times. The impact of the number of anode infiltrations is shown in (c) peak power vs. temperature, and (d) components of the AC impedance spectra at 700°C.

TOC

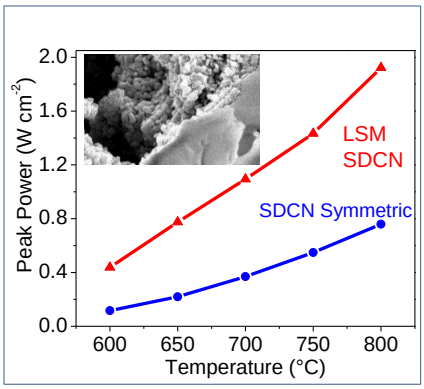
Peak Power (W cm-2)
2.0
1.6
1.2
0.8
0.4
0.0
600
650
700
750
800
Temperature (°C)
LSM
SDCN
SDCN Symmetric